Journal of Nuclear Materials 399 (2010) 212–218

Contents lists available at ScienceDirect

Journal of Nuclear Materials

journal homepage: www.elsevier.com/locate/jnucmat

Corrosion behavior of plasma-sprayed Al_2O_3–Cr_2O_3 coatings in hot lithium molten salt

Soo Haeng Cho *, Sung Bin Park, Dae Seong Kang, Myeong Soo Jeong, Heong Park, Jin Mok Hur, Han Soo Lee

Korea Atomic Energy Research Institute, 1045 Daedeokdaero Yuseong-gu, Daejeon 305-353, Republic of Korea

ARTICLE INFO

Article history:
Received 5 August 2009
Accepted 25 January 2010

Keywords:
Plasma coating
Al_2O_3–Cr_2O_3 top coat
Hot corrosion
Electrolytic reduction
Structural material

ABSTRACT

In this study, hot corrosion studies were performed on bare as well as coated superalloy specimens after exposure to molten lithium chloride environment at 675 °C for 216 h under an oxidizing atmosphere. The substrates of the IN713LC superalloy specimens were sprayed with an aluminized NiCrAlY bond coat and then with an Al_2O_3–Cr_2O_3 top coat. The as-coated and tested specimens were examined by optical microscopy (OM), scanning electron microscopy (SEM)/X-ray energy dispersive spectrometry (EDS) and X-ray diffraction (XRD), respectively. The bare superalloy reveals an obvious weight loss, and the scale formed on the surface of the bare superalloy was spalled due to the rapid scale growth and thermal stress. The top coatings showed a much better hot corrosion resistance in the presence of LiCl–3 wt.% Li_2O molten salt when compared with those of the uncoated superalloy and the aluminized bond coatings. These coatings have been found to be beneficial for increasing to the hot corrosion resistance of the structural materials for handling high temperature lithium molten salts.

1. Introduction

Molten salt technology has been widely applied in the industrial world because of its physical and chemical characteristics, in particular its high electrical conductivity, high processing rate, fluid features, etc. Molten salts can cause corrosion to the container materials and other accessories used in the construction of various equipments. Therefore, studies on the corrosion of the equipment and the structural materials for handling high temperature molten salts have also been continuously carried out. Superalloys have been developed for high temperature application [1–4]. However, these alloys may not be able to meet both the high temperature strength requirements and high temperature corrosion resistance simultaneously. So, a coating of thermal barrier type has been found to be the most effective and economical method to enhance the corrosion resistance at an elevated temperature without destroying the mechanical properties of a substrate. The top coating materials for the thermal barrier are generally composed of Al_2O_3–Cr_2O_3, CeO_2, MgO or Y_2O_3 stabilized ZrO_2, and bond coat is applied between a substrate and top coat to enhance an adhesion [5–11].

In recent R&D studies, pyrochemical processes have received much attention as alternatives for the treatment of spent oxide nuclear fuels when compared to hydrometallurgical processes. Argonne National Laboratory (ANL) has been developing pyrochemical technologies based on a molten salt system [12,13].

In this study, the electrolytic reduction of spent oxide fuel involves the liberation of oxygen in a molten LiCl electrolyte, which results in a chemically aggressive environment that is too corrosive for typical structural materials [12]. Therefore, for an implementation of the electrolytic reduction technology, corrosion resistant materials should be developed. However, few reports are found on the corrosion resistance of the structural materials for handling a hot lithium molten salt.

In this work, a plasma-sprayed NiCrAlY bond coat and Al_2O_3–Cr_2O_3 top coat were selected due to the excellent resistance to erosion and thermal difference [14–17]. The hot corrosion behaviors of an aluminized NiCrAlY and Al_2O_3–Cr_2O_3 coated IN713LC in the presence of lithium molten salt have been investigated under simulated electrolytic reduction conditions.

2. Experimental

The substrates were 70 mm × 15 mm × 2 mm specimens of superalloy IN713LC (Ni: 74.0, Cr: 11.57, Fe: 0.10, C: 0.05, Si: 0.02, Mo: 4.15, Al: 6.05, Co: 0.08, Ti: 0.76, Nb: 1.95 wt.%), which were degreased and sand-blasted (Al_2O_3, 60 mesh) before spraying. Table 1 indicates the characteristics of the coating materials and the parameters of the plasma spraying are listed in Table 2. The NiCrAlY bond coat provides a rough surface for mechanical bonding of the

* Corresponding author. Tel.: +82 42 868 2584; fax: +82 42 868 2053.
E-mail address: nshcho1@kaeri.re.kr (S.H. Cho).

0022-3115/$ - see front matter © 2010 Elsevier B.V. All rights reserved.
doi:10.1016/j.jnucmat.2010.01.022

Table 1
Characteristics of the coating materials.

Layer	Product	Composition (wt.%)	Process	Thickness (μm)
Top coat	METCO	Al_2O_3–50Al_2O_3	Air plasma spray (APS)	200–250
Bond coat	AMDRY, 965	Ni–22Cr–10Al–0.1Y	–	100–150

Table 2
Parameters of plasma spraying.

Parameters	Contents
Apparatus model	METCO-9MC
Plasma gas	Ar/H_2
Gun-to-work distance (mm)	125
Gun traverse rate (cm/s)	20
Gas pressure (CFH)	Ar: 80, H_2: 20
Powder feed rate (g/min)	40
Arc current (A)	600
Arc voltage (V)	78

ceramic top coat, protects the underlying alloy substrate against high temperature corrosion and minimizes the effect of coefficient of thermal expansion mismatch between the substrate and the ceramic top coat materials. Aluminizing was introduced to increase the Al content on the coating layer [14,17]. For the aluminizing, the specimens with Al(2.0%)–Cr(3.0%)–Al_2O_3(94.9%)–NH_4F(0.1%) mixed powders were placed inside a stainless steel coating box. About a 30–50 μm thickness aluminum diffusion layer was formed under a hydrogen atmosphere at 1052 ± 14 °C for 2 h. The air

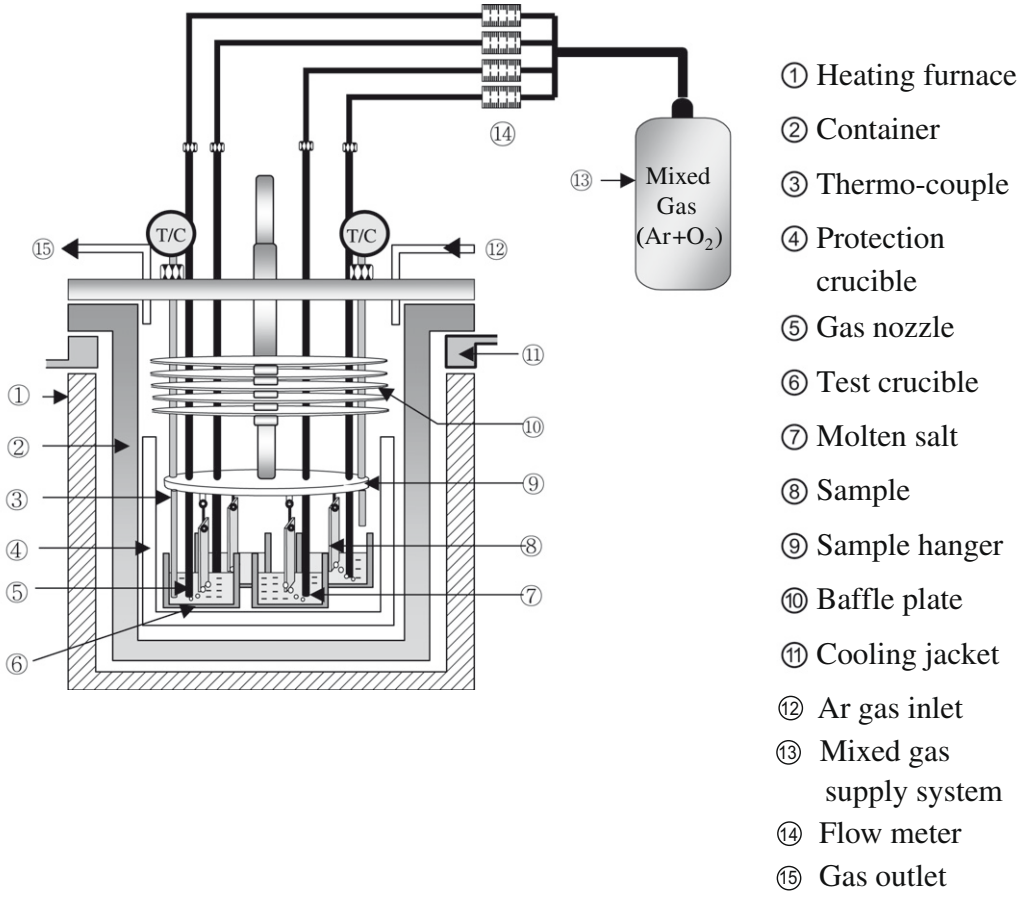

Fig. 1. Schematic diagram of the apparatus for the corrosion test.

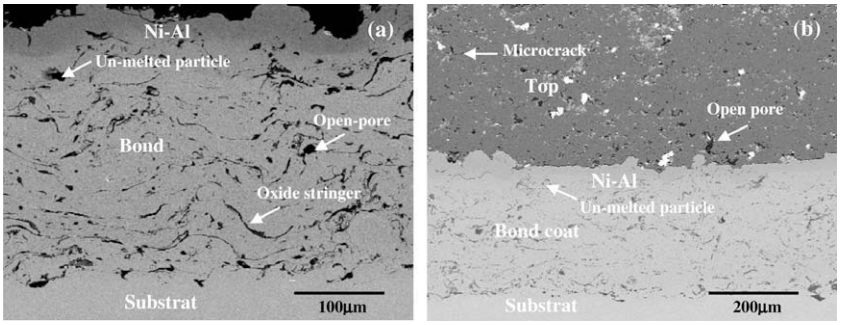

Fig. 2. Morphologies in cross-section of aluminized NiCrAlY (a) and aluminized NiCrAlY–Al_2O_3–Cr_2O_3 and (b) coated IN713LC.

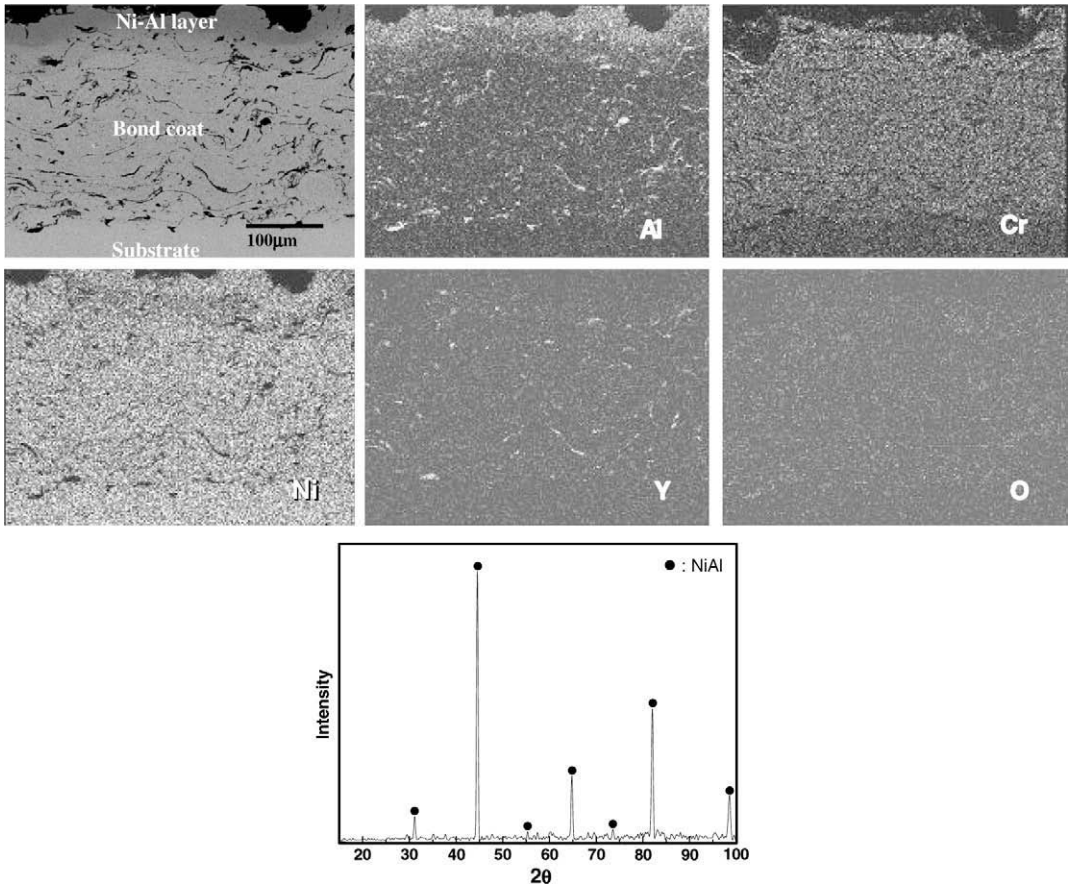

Fig. 3. Cross-sectional SEM image, elemental distribution and XRD pattern of aluminized NiCrAlY coated IN713LC.

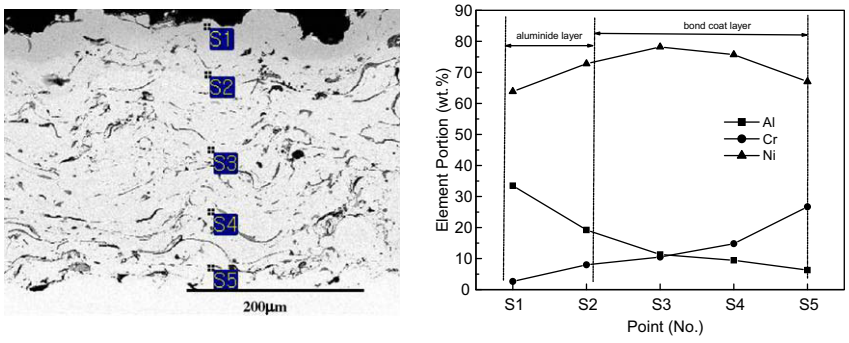

Fig. 4. Cross-sectional SEM image and point quantitative analysis of aluminized NiCrAlY coated IN713LC.

plasma-sprayed Al_2O_3–Cr_2O_3 layer acts as a corrosion resistant thermal barrier. The experimental apparatus is shown in Fig. 1. A LiCl–Li_2O molten salt was introduced into a dense MgO crucible and then heated at 300 °C for 3 h in an argon atmosphere to remove any possible remaining moisture. After reaching the set conditions, the specimens and alumina tube were immersed into the molten salt, and mixed gas (Ar–10%O_2) was supplied through an alumina tube. The corrosion tests were carried out at 675 °C and for 216 h. The Li_2O concentration in LiCl was 3 wt.%. Following the corrosion test, the specimens were withdrawn from the salt and kept under an argon gas atmosphere while the furnace was cooled down to room temperature. Before and after the corrosion test, the specimens were ultrasonically cleaned in acetone. Initial weight and final weight of the specimens exposed to the molten salt were taken to assess the corrosion. After the tests, the corroded specimens were cut by a diamond cutter and ultrasonically cleaned in acetone for characterization purposes. Some specimens were prepared for metallographic examination by cold-mounting, grinding and polishing. Optical microscopy was used to examine the penetration of molten salt into coatings. The microstructure, morphology and chemical composition of the surface and the cross-section of the coatings were examined by SEM (scanning electron microscopy, JEOL, JSM-6300) equipped with energy dispersive spectrometer (EDS). XRD (X-ray diffraction, Rigaku, DMAX/1200) was used to determine the structure of the coatings and hot corrosion products. The coating porosity was characterized by means of the surface image analyzer, OLYMPUS BX60M.

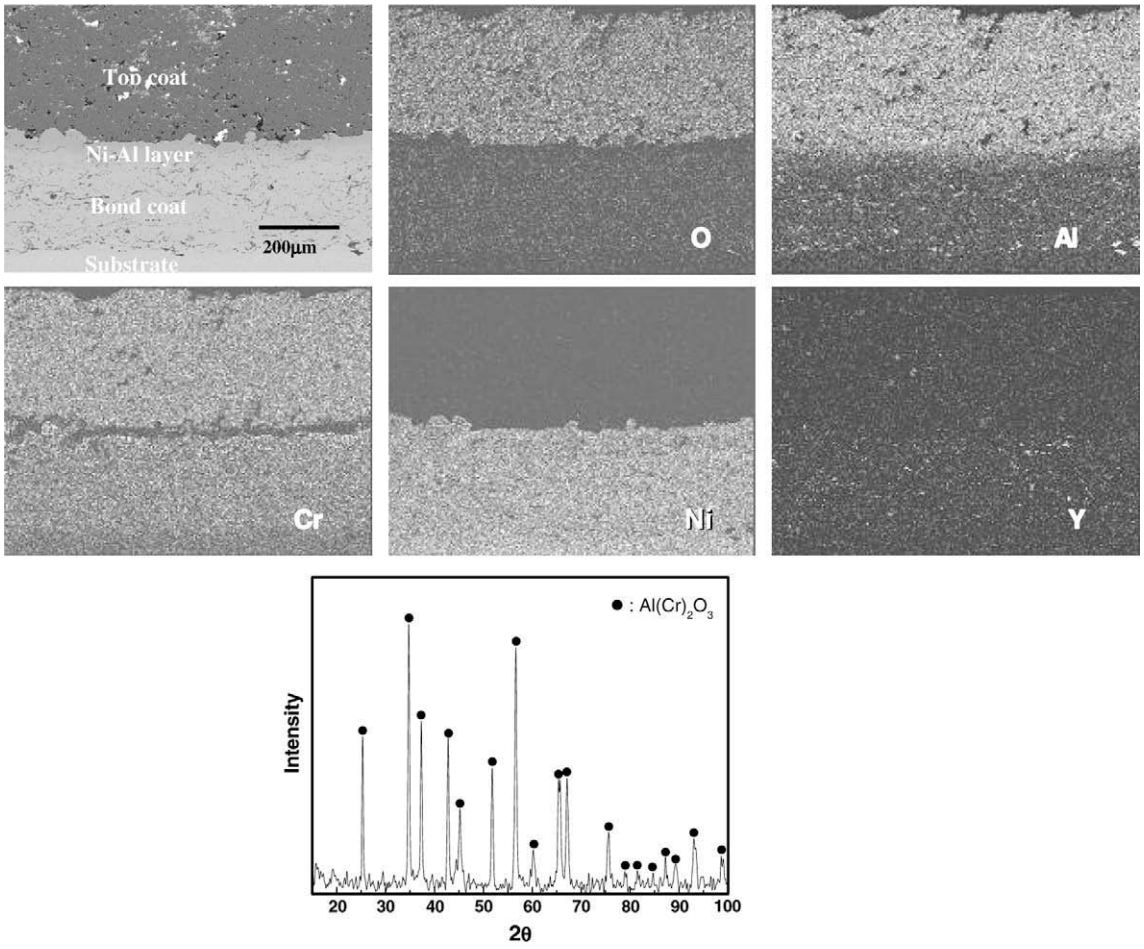

Fig. 5. Cross-sectional SEM image, elemental distribution and XRD pattern of aluminized NiCrAlY–Al_2O_3–Cr_2O_3 coated IN713LC.

3. Results and discussion

3.1. Microstructure of the coatings before corrosion

Fig. 2 shows the cross-sections of the aluminized bond coat (Fig. 2a) and the aluminized bond and top coat (Fig. 2b) obtained by plasma spraying. Aluminized NiCrAlY and Aluminized NiCrAlY/Al_2O_3–Cr_2O_3 systems were both successfully deposited by plasma spraying, using the parameters in Table 2. As shown in Fig. 2a, the aluminized bond coat showed a lamellar structure which is a characteristic of plasma-sprayed coating, including pores, unmelted particles and oxide inclusions [14–17]. The as-sprayed microstructure of the top coat exhibited imperfections such as pores and microcracks which are a complex function of the spraying parameters (Fig. 2b) [9,14,15]. The porosity of the coatings using an image analyzer has been found to be in the range 5.5 ~ 7.5%. Fig. 3 shows the cross-sectional SEM image and the elemental distribution and the XRD pattern of aluminized NiCrAlY coated IN713LC. A cross-sectional microstructure of the (Ni, Cr)-rich region and NiAl–aluminide layer is shown in Fig. 3. According to XRD the phase composition of the Ni–Al layer consisted of NiAl (Fig. 3). The cross-sectional SEM image and the point quantitative analysis of aluminized NiCrAlY coated IN713LC is shown in Fig. 4. In the outer layer (aluminide layer), the Al content is about 34 wt.% and a small amount of Cr can also be detected. In the inner layer, the average content of Al element is 13 wt.%, a little higher than in the original plasma coating. Fig. 5 shows the cross-sectional SEM image and the elemental distribution and the XRD pattern of aluminized NiCrAlY and Al_2O_3–Cr_2O_3 coated IN713LC. According to XRD results $Al(Cr)_2O_3$ is the main phase of the outer layer. The Al_2O_3–Cr_2O_3 system is a continuous solid solution in which the solute is completely incorporated in the lattice [18]. Hence, it shows a single phase X-ray diffraction pattern of $Al(Cr)_2O_3$. The only difference in the X-ray diffraction patterns is that the location of peaks is

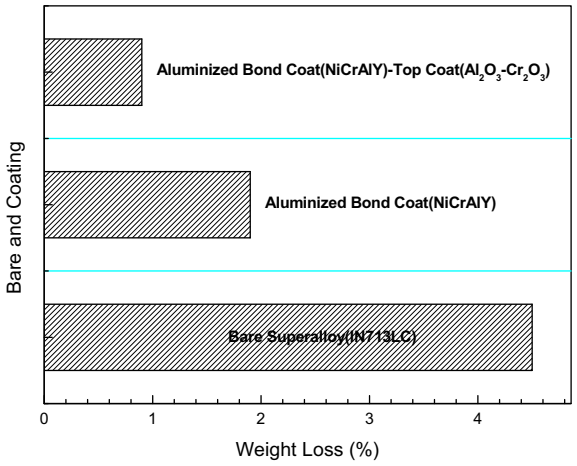

Fig. 6. Weight losses of the bare and aluminized bond and top coated IN713LC corroded at 675 °C for 216 h.

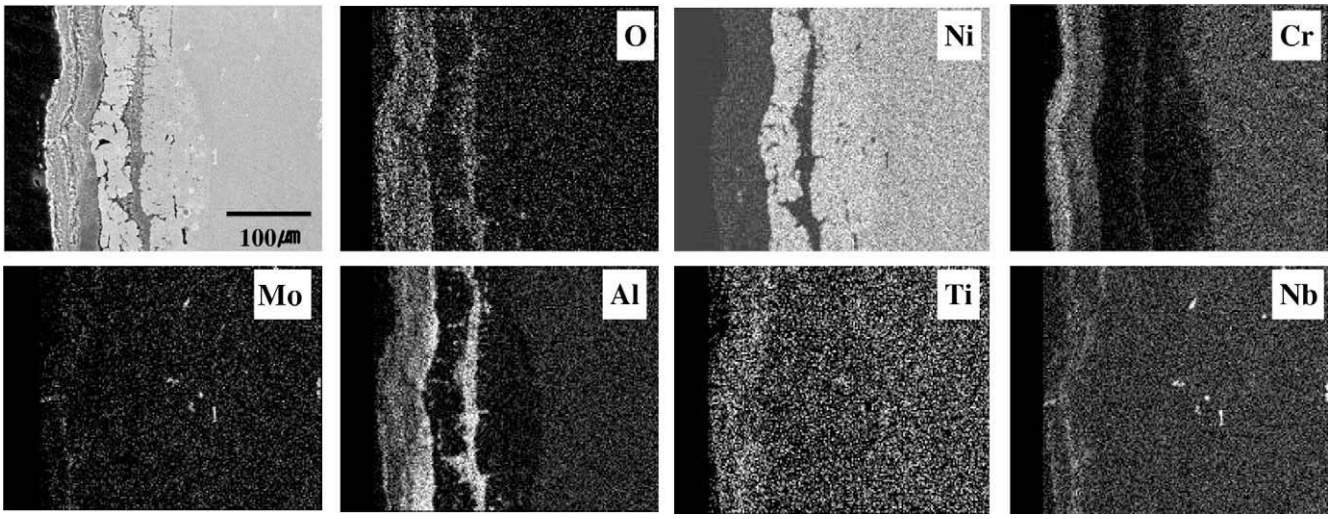

Fig. 7. Cross-sectional SEM image and the elemental distribution of bare IN713LC corroded at 675 °C for 216 h.

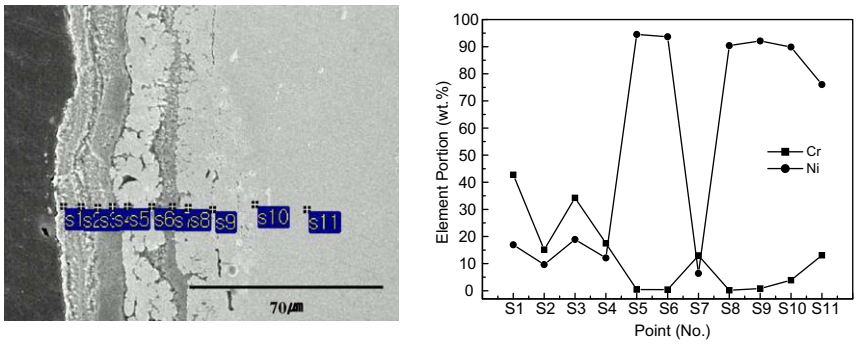

Fig. 8. Cross-sectional SEM image and point quantitative analysis of bare IN713LC corroded at 675 °C for 216 h.

shifted due to expansions of the lattices. Fig. 5 also shows a cross section of the plasma spray coating layer which is identified by a triple-layer structure consisting of (Ni,Cr)-rich region, (Al_2O_3–Cr_2O_3)-rich region and aluminide layer.

3.2. Mass loss

The weight losses of the bare IN713LC and its coated specimens after the corrosion tests in a LiCl–Li_2O molten salt at 675 °C are shown in Fig. 6. After a 216 h hot corrosion, the bare superalloy reveals an obvious weight loss. Under a high temperature oxidative molten salt environment, the reason for the weight loss with time was attributed to spallation of the scale formed on the surface of the bare specimen due to the rapid scale growth and thermal stress [17]. On the other hand, the low weight change of the specimen with top coat by thermal barrier type seems to be attributed to a superior protection ability and thermal stability in a hot lithium molten salt system [10].

3.3. Corrosion behavior

3.3.1. Bare superalloy

The cross-sectional SEM image and elemental distribution of the bare IN713LC corroded for 216 h are shown in Fig. 7. As shown in Fig. 7, the scale was mainly composed of TiO_2, Cr_2O_3, and Al_2O_3. It is a typical appearance of hot corrosion, porous oxide, internal oxidation, and an alloy depleted layer [16]. The elemental distribution shows the outer scale mainly composed of TiO_2 and Al_2O_3, and intermediate layer rich in chromium, and an Al_2O_3 scale formed close to the substrate. The oxygen active elements such as Al and Ti were preferentially oxidized and participated in the corrosion layer [19]. A depleted zone of Cr beneath the oxide/metal interface has been observed. Below about 10% Cr, these areas lose resistances and are corroded preferentially [20]. The Cr content in the Cr depleted area was measured 0.43 wt.% (S5), 0.41 wt.% (S6), 0.17 wt.% (S8), 0.79 wt.% (S9) and 3.88 wt.% (S10) as shown in Fig. 8.

3.3.2. Aluminized bond coat

Fig. 9 shows the cross-sectional SEM image and the elemental distribution and the XRD pattern of aluminized NiCrAlY coated IN713LC corroded at 675 °C for 216 h. The SEM image mapping analysis results show that Cr is present in the Ni–Al aluminide layer. From the result on the as aluminized bond coat, the aluminide layer should be Cr free area (Fig. 3). This result can be interpreted by the formation of a Cr depleted area in the bond coating layer. This means that Cr diffused to Ni–Al aluminide layer from the bond coating layer due to its superior chemical affinity with Li_2O in molten salt. Thus Cr was shown to be present at the Ni–Al aluminide layer which did not have Cr before the corrosion test. It should be noted the most of the Ni is eliminated at the aluminide layer with traces of Ni found on the surface and discontinuous Ni concentration in the bond coating layer. This also may imply that Ni also was dissolved by molten salt while basic fluxing [21]. XRD result shows that the surface is mainly composed of LiAl(Cr)O_2 solid solution formed by the chemical reaction between

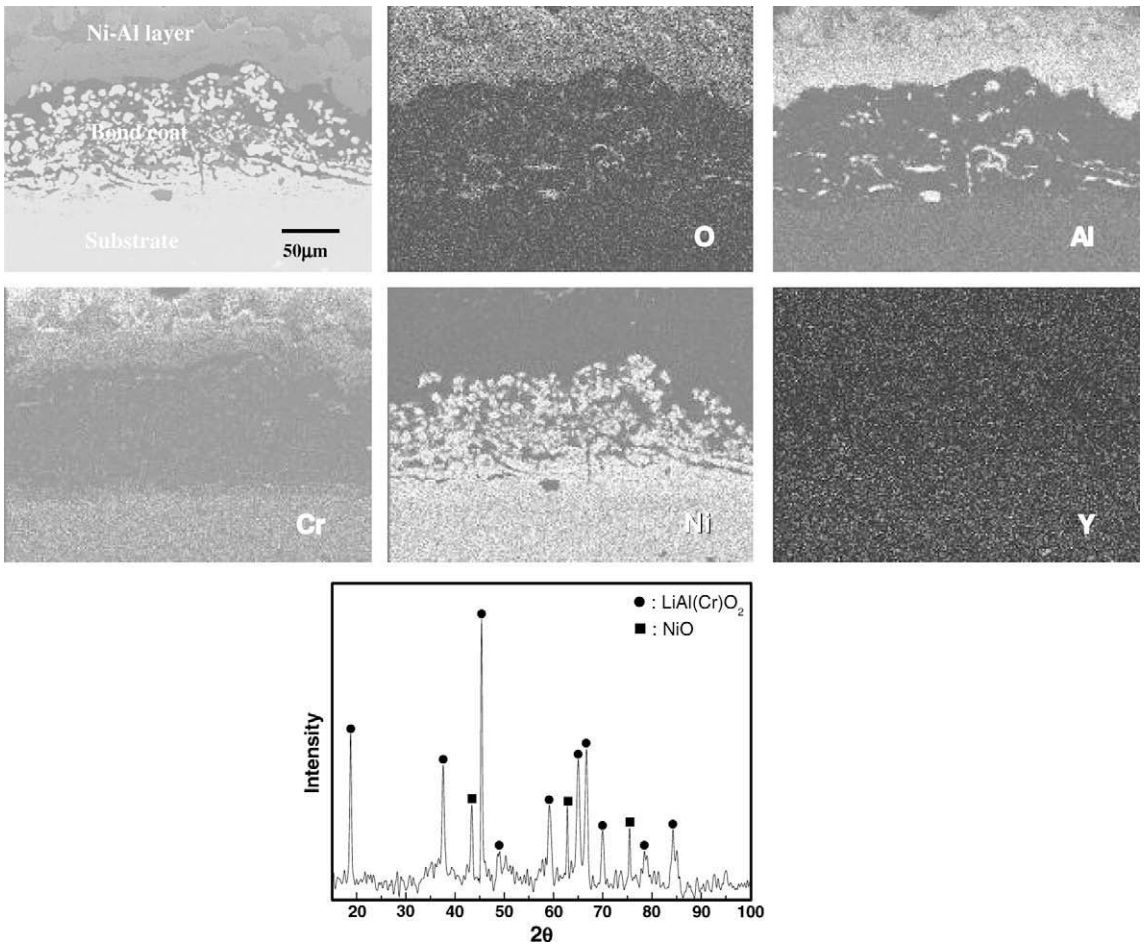

Fig. 9. Cross-sectional SEM image, elemental distribution and XRD pattern of aluminized NiCrAlY coated IN713LC corroded at 675 °C for 216 h.

Al_2O_3–Cr_2O_3 solid solution and Li_2O [18], whereas NiO is mixed as a second phase without solution. Also, a small amount of NiO remained at the surface due to considerable dissolution into the molten salt. Hence, the weight loss is attributed to the dissolution of this main component. The formation of a dense and continuous $LiAl(Cr)O_2$ phase in the outer layer retards internal diffusion of oxygen ions. The enrichment of Ni at the interface between bond coat and substrate was observed (Fig. 9). Ni is an element that prevents the internal diffusion of an oxygen ion by its accumulation at the interface of an oxide/oxide or beneath oxide layers [22,23]. Hence, the weight loss of the specimen with aluminized bond coat is 58% less than that of bare alloy as shown in Fig. 6. As shown in Fig. 9, the formation of pores in the interface may be due to the Kirkendall effect caused by Cr diffusion [24].

3.3.3. Aluminized bond and top coat

Fig. 10 shows the cross-sectional SEM image and the elemental distribution and the XRD pattern of aluminized NiCrAlY and Al_2O_3–Cr_2O_3 coated IN713LC corroded at 675 °C for 216 h. The cross section of plasma spray coating layer is identified as a triple-phase structure consisting of (Ni,Cr)-rich region, and (Al_2O_3, NiO)-rich region, (Al_2O_3–Cr_2O_3)-rich region. SEM image mapping result shows that Al, Cr and O are dispersed at the surface layer, and Cr is found to be depleted. It seems that the Al_2O_3–Cr_2O_3 solid solution reacted with Li_2O in molten LiCl [18], and the crystal structure is believed to be $LiAl(Cr)O_2$ in which the X-ray diffraction peaks are shifted due to lattice distortion by the solute dissolution. The formation of such an $LiAl(Cr)O_2$ phase would be a primary factor of weight loss due to the solubility to molten LiCl. However, the components such Al, Cr and Ni were well preserved after corrosion test, which means the top coating layer effectively served as a diffusion barrier. Also, a dense, continuous and protective top coat retards the internal diffusion of oxygen as well as external diffusion of the alloying elements from the metallic bond coat, hence, it seems that the substrate was protected from the internal oxidation. The superior corrosion resistance of the specimen with the top coat should be attributed to the chemical and thermal stability and the superior protection ability. Also, the aluminized bond and top coat possesses a better corrosion resistance than the aluminized bond coat alone [9].

4. Conclusion

The mass loss was in the order of aluminized bond and top coat < aluminized bond coat < bare superalloy (IN713LC). The phase composition of the aluminized bond coat surface corroded at 675 °C for 216 h consisted of $LiAl(Cr)O_2$ and NiO, and that of the aluminized bond and top coat surface was shown $LiAl(Cr)O_2$. Compared with the bare superalloy (IN713LC), the aluminized bond and top coat showed a much better hot corrosion resistance in the presence of LiCl–Li_2O molten salt as a result of the formation of a dense, continuous and protective $LiAl(Cr)O_2$ layer. The superior corrosion resistance of the specimen with the top coat should be attributed to both the chemical and thermal stability and the superior protection ability due to retarding the external diffusion of the alloying elements from the metallic bond coat. Also, the low mass

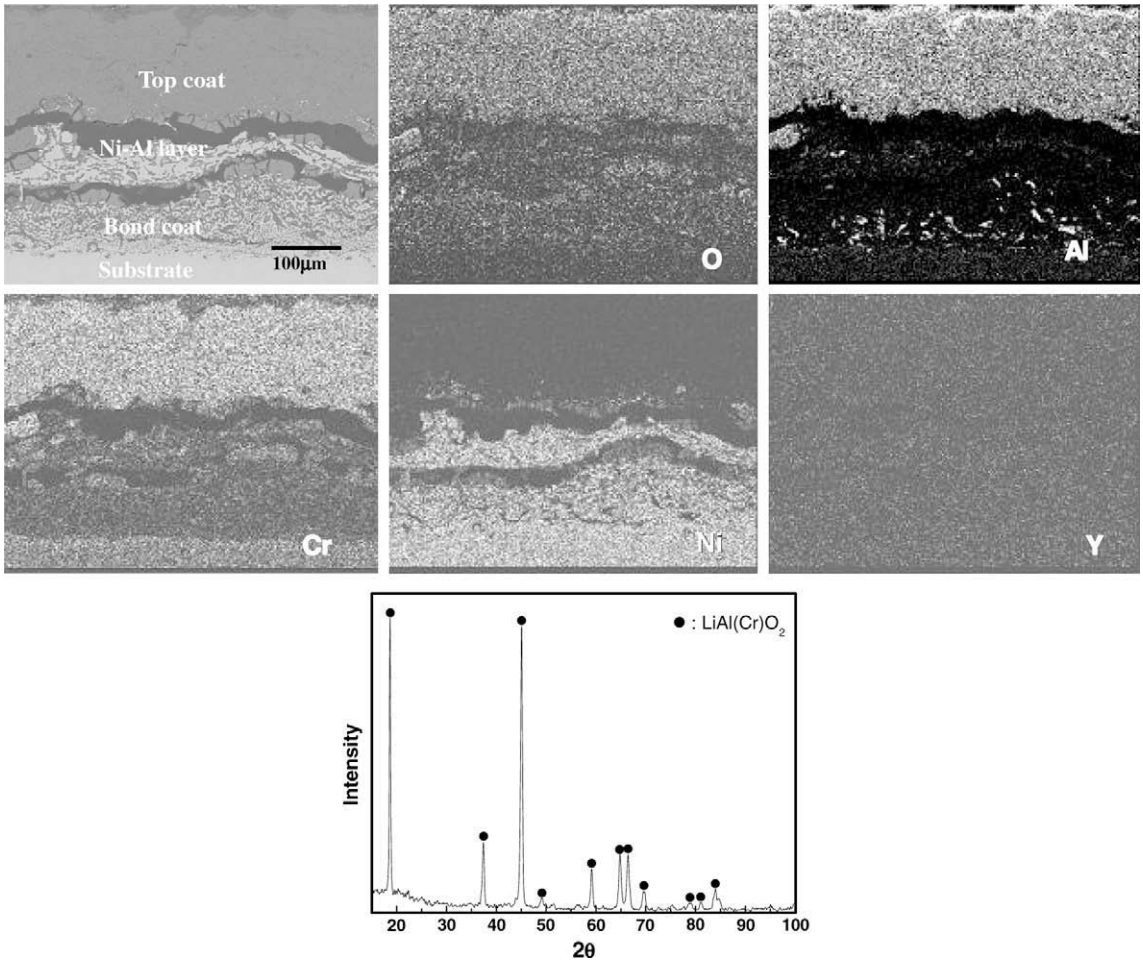

Fig. 10. Cross-sectional SEM image, elemental distribution and XRD pattern of aluminized NiCrAlY–Al_2O_3–Cr_2O_3 coated IN713LC corroded at 675 °C for 216 h.

loss of the specimen with top coat demonstrates that the top coat played important role as a protective layer.

Acknowledgments

This work was supported by Nuclear Research & Development Program of the Korea Science and Engineering Foundation (KOSEF) grant funded by the Korean government (MEST). (Grant Code: M20703030001-08M0303-00110).

References

[1] T. Ishitsuka, K. Nose, Corros. Sci. 44 (2002) 247.
[2] B.P. Mohanty, D.A. Shores, Corros. Sci. 46 (2004) 2893.
[3] F. Colom, A. Bodalo, Corros. Sci. 12 (1972) 73.
[4] A. Ruh, M. Spiegel, Corros. Sci. 48 (2006) 679.
[5] B. Wang, C. Sun, J. Gong, R. Huang, L. Wen, Corros. Sci. 46 (2004) 519.
[6] Q.M. Wang, Y.N. Wu, P.L. Ke, H.T. Cao, J. Gong, C. Sun, L.S. Wen, Surf. Coat. Technol. 186 (2004) 389.
[7] R. Mobarra, A.H. Jafari, M. Karaminezhaad, Surf. Coat. Technol. 201 (2006) 2202.
[8] B.S. Sidhu, S. Prakash, Surf. Coat. Technol. 166 (2003) 89.
[9] Y.N. Wu, P.L. Ke, Q.M. Wang, C. Sun, F.H. Wang, Corros. Sci. 46 (2004) 2925.
[10] A.R. Shankar, U.K. Mudali, R. Sole, H.S. Khatak, B. Raj, J. Nucl. Mater. 372 (2008) 226.
[11] M.A. Uusitalo, P.M.J. Vuoristo, T.A. Mantyla, Corros. Sci. 46 (2004) 1311.
[12] J.E. Indacochea, J.L. Smith, K.R. Litko, E.J. Karell, A.G. Raraz, Oxid. Metal 55 (2001) 1.
[13] E.J. Karell, R.D. Pierce, T.P. Mulcahey, ANL/CMT/CP-89562, 1996.
[14] X. Ren, F. Wang, Surf. Coat. Technol. 201 (2006) 30.
[15] L. Zhao, M. Parco, E. Lugscheider, Surf. Coat. Technol. 179 (2004) 272.
[16] M.H. Guo, Q.M. Wang, P.L. Ke, J. Gong, C. Sun, R.F. Huang, L.S. Wen, Surf. Coat. Technol. 200 (2006) 3942.
[17] C.H. Koo, C.Y. Bai, Y.J. Luo, Mater. Chem. Phys. 86 (2004) 258.
[18] E.N. Bunting, Phase Diagrams for Ceramists, in: K. Reser (Ed.), American Ceramic Society, Ohio, 1964, p. 121.
[19] E.T. Turkdogan, Physical Chemistry of High Temperature Technology, Academic Press, New York, 1980.
[20] D.A. Jones, Principles and Prevention of Corrosion, Macmillan Publishing Company, New York, 1992.
[21] R.A. Rapp, Corros. Sci. 44 (2002) 209.
[22] G.C. Wood, Corros. Sci. 2 (1962) 173.
[23] S.H. Cho, J.M. Hur, C.S. Seo, S.W. Park, J. Alloys Compd. 452 (2008) 11.
[24] A.M. Karlsson, A.G. Evans, Acta Mater. 49 (2001) 1793.